

pubs.acs.org/JACS Article

# Elucidating Electric Field-Induced Rate Promotion of Brønsted Acid-Catalyzed Alcohol Dehydration

Bhavish Dinakar, Karl S. Westendorff, Juan F. Torres, Mostapha Dakhchoune, Katelyn Groenhout, Nathan Ewell, Yogesh Surendranath,\* Mircea Dincă,\* and Yuriy Román-Leshkov\*



Cite This: https://doi.org/10.1021/jacs.5c05891



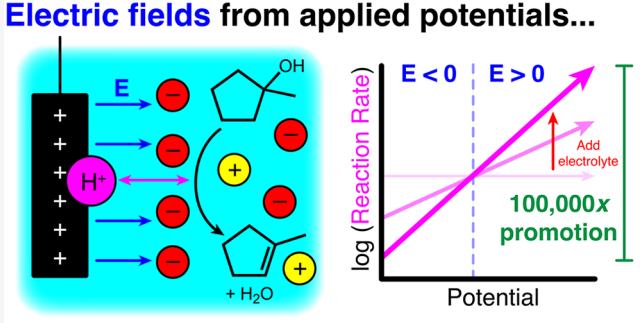
**ACCESS** I

III Metrics & More

Article Recommendations

s Supporting Information

ABSTRACT: Applied potentials have been demonstrated as a powerful tool to promote heterogeneous Brønsted acid catalysis by orders of magnitude, leveraging interfacial electric fields to stabilize protonated intermediates. However, the use of flat two-dimensional electrodes with inherently low active site densities limits the application of conventional thermochemical characterization techniques that can probe the nature of catalytic active sites. Here, we use kinetic analyses with an electrostatics-based model to elucidate the intricacies of potential-induced rate promotion, employing liquid-phase dehydration of 1-methylcyclopentanol catalyzed by carboxylic acid groups on carbon nanotubes as a probe system. Using a basket electrode to directly polarize catalyst powder, we demonstrate that thermocatalytic reaction rates can be



... control thermochemical rate promotion

promoted by 100,000-fold, exhibiting a log—linear dependence on applied potential with rate-potential scalings as high as  $125 \pm 4$  mV per 10-fold rate increase. In agreement with model predictions, we show that lower ionic strengths attenuate potential sensitivity, resulting from a weakening of the interfacial electric field that interacts with the acidic proton. Furthermore, we experimentally confirm the model-predicted "isokinetic potential" (at  $\sim 0.6$  V vs Ag/AgCl)—the potential at which all rate scaling lines at various ionic strengths intersect, making the rate independent of ionic strength. Base titrations reveal that only  $\sim 8\%$  of the carboxylic acid sites are catalytically active, yet these same active sites are operational at the highest and lowest potentials. Collectively, our results provide a key methodology for modeling catalytic effects of electric fields, quantifying active sites under applied potential, and demonstrating fundamental principles of electric field-induced rate promotion.

## **■ INTRODUCTION**

Catalysts play an important role in accelerating chemical processes. However, achieving high activity often requires operating at high temperatures and pressures. These conditions increase operational costs and safety risks, making it desirable to investigate alternative strategies for enhancing catalytic activity under milder conditions.<sup>1</sup>

In enzymatic catalysis, charged functional groups near enzyme active sites generate strong, oriented electric fields that stabilize charge-separated transition states, increasing reaction rates by orders of magnitude. Inspired by this principle, the use of electric fields has emerged as a tool to improve catalyst performance under milder conditions. Indeed, studies have shown that generating an electric field, by applying a potential in scanning tunneling microscope reactors or by installing charged groups on molecules, leads to significant changes in reactivity in agreement with computational predictions. While these methods provide proof-of-concept demonstrations, they are difficult to scale for practical heterogeneous catalysts due to the

complexity of the reactor system or the often unknown active site structure in heterogeneous catalysis. <sup>18</sup>

To address this challenge, studies have explored using electrochemical cells with liquid-phase reactions conducted in electrolyte solutions, taking advantage of the strong ( $\sim$ 0.1 V/nm) electric fields that occur at electrode/electrolyte interfaces. In these systems, a working electrode (WE) coated with a catalyst is biased relative to a reference electrode (RE), with the excess charge for the WE balanced by an inert counter electrode (CE). The resulting interfacial electric field extends from the WE surface into the electrolyte solution, affecting the energetics of reactive intermediates and transition states.

Several studies have demonstrated that applied potential can modulate reaction rates and selectivity in liquid-phase

Received: April 7, 2025 Revised: June 20, 2025 Accepted: June 23, 2025



thermochemical reactions, including olefin isomerization, <sup>19</sup> hydrazine<sup>20</sup> and hydrogen oxidation, <sup>21</sup> carbon dioxide<sup>22,23</sup> and ethylene hydrogenation, <sup>24,25</sup> epoxide isomerization, <sup>26</sup> and intramolecular carbene reactions.<sup>27</sup> However, many of these studies attribute rate promotion to alternative phenomena such as proton spillover, 19 local pH changes, 23 electrochemically generated promoting species, 28 or specific interactions with electrolyte, 21 rather than direct electric field effects. For cases in which electric fields are invoked to explain rate enhancements, the origin of the promotional effect remains unclear, as it is difficult to discern how the electric field interacts with the active site and why the electric field application should lead quantitatively to the observed rate/selectivity alteration. 25,26,29 Furthermore, these systems are relatively insensitive to applied potential, requiring large potential changes (0.2-10 V) to obtain 10-fold rate increases.

Recently, our groups reported that Brønsted acid-catalyzed alcohol dehydration (a thermochemical reaction that is not expected to occur from two electrochemical half-reactions) is particularly sensitive to applied potential.<sup>24</sup> For both phosphotungstic acid supported on carbon paper (PTA/C) and Ti foil (with surface titanols hypothesized to be the active site), dehydration of 1-methylcyclopentanol to 1-methylcyclopentene exhibited an exponential rate increase with applied potential, with rate-potential scalings of 70-100 mV per 10fold rate increase. This observed rate promotion was hypothesized to originate from the interfacial electric field formed at the WE/electrolyte interface (Figure 1A), where applying a positive potential bias accumulates positive surface charges on the WE, creating an electric field between the WE surface and charge-balancing anions in the electrolyte. This electric field creates an electrostatic driving force that promotes the protonation of the substrate, effectively increasing the active site acidity and thus increasing the reaction rate.

Despite these promising results, verifying certain mechanistic aspects of electric field-driven catalysis has been challenging, largely due to the use of flat two-dimensional (2D) electrodes (Figure 1B). Although the potential of these electrodes can be conveniently controlled via a potentiostat, their low surface areas result in a small density of active sites, limiting measurable product yields to high applied potentials (>1.2 V vs Ag/AgCl).<sup>24</sup> At such high potentials, the leakage current can become significant, raising the possibility that electrochemically generated H<sup>+</sup> may contribute to the observed rate enhancement. Furthermore, batch-to-batch variation in 2D electrode preparation from dropcasting<sup>30–32</sup> and the inability to measure kinetics without applied potential make it difficult to characterize active sites, count their density, and determine whether all sites are promoted equally with applied potential.<sup>24</sup> As such, our prior work only reported upper-bound estimates for site densities using geometric arguments or assumptions that all added acid sites are equally active.<sup>24</sup>

Here, we show that three-dimensional (3D) basket electrodes provide an effective platform for directly polarizing conductive, porous catalyst powders, overcoming the limitations previously imposed by flat 2D electrodes (Figure 1B). Using carboxylic acid-functionalized carbon nanotubes as highsurface-area Brønsted acid catalysts, we demonstrate that alcohol dehydration rates can be controllably promoted by 100,000-fold under applied potential. This large range of rate control enabled us to perform site-counting base titrations coupled with rate demotion studies, revealing that all active

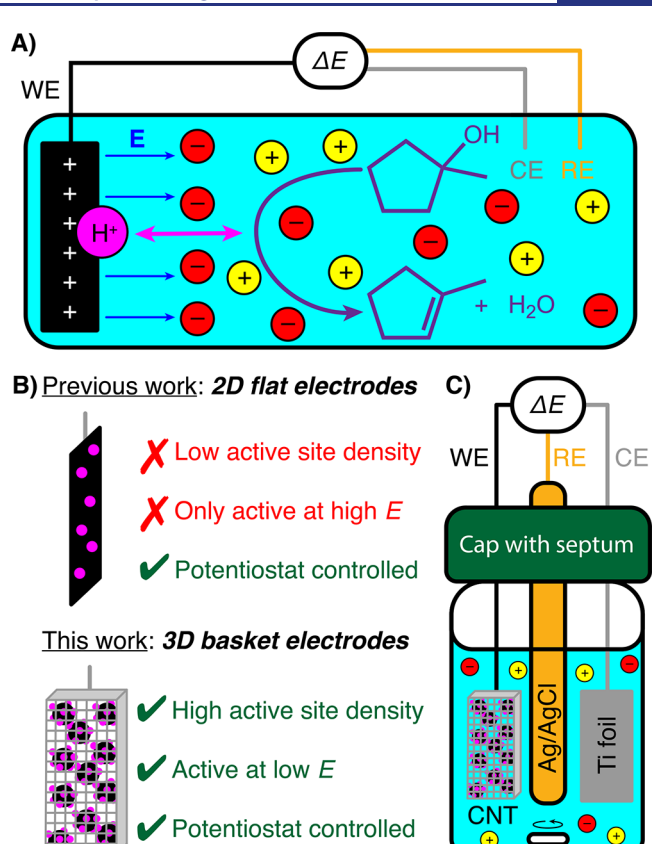


Figure 1. (A) Diagram of electric field-induced Brønsted acidcatalyzed alcohol dehydration of 1-methylcyclopentanol to 1methylcyclopentene. A potential ( $\Delta E$ ) is applied between the catalytic working electrode (WE) and reference electrode (RE), with charge supplied from an inert counter electrode (CE). The applied potential generates a strong electric field E between the WE and electrolyte ions in solution, changing the catalyst acidity and altering the reaction rate. (B) Comparison of this work (using 3D basket electrodes) to previous liquid-phase electric field-induced catalysis (using 2D flat electrodes). (C) Diagram of experimental setup for electric fieldinduced alcohol dehydration with a basket electrode. The WE (consisting of carboxylic acid-functionalized carbon nanotubes, denoted CNT, contained within a stainless steel (SS) mesh basket electrode) is connected via a potentiostat to a Ag/AgCl RE and Ti foil CE in a stirred septum-capped 20 mL glass vial containing an electrolyte solution.

sites experience uniform electric field enhancement and that the promotion primarily results from electric fields rather than electrochemical H<sup>+</sup> generation from stray Faradaic current. Furthermore, by systematically changing electrolyte concentration, we experimentally demonstrate the existence of an "isokinetic potential" (IKP)—the hypothesized potential at which the reaction rate becomes independent of electrolyte concentration—further validating our mechanistic model of electric field-promoted Brønsted acid catalysis.

# ■ RESULTS AND DISCUSSION

Design of Basket Reactor Electrodes for Non-Faradaic Promotion of Carbon Nanotube Catalysts. To investigate the origin of the non-Faradaic promotion of Brønsted acid-catalyzed alcohol dehydration, we sought to identify a suitable electrically conductive heterogeneous Brønsted acid catalyst with a high acid site density to conduct mechanistic studies, as previously used 2D electrodes

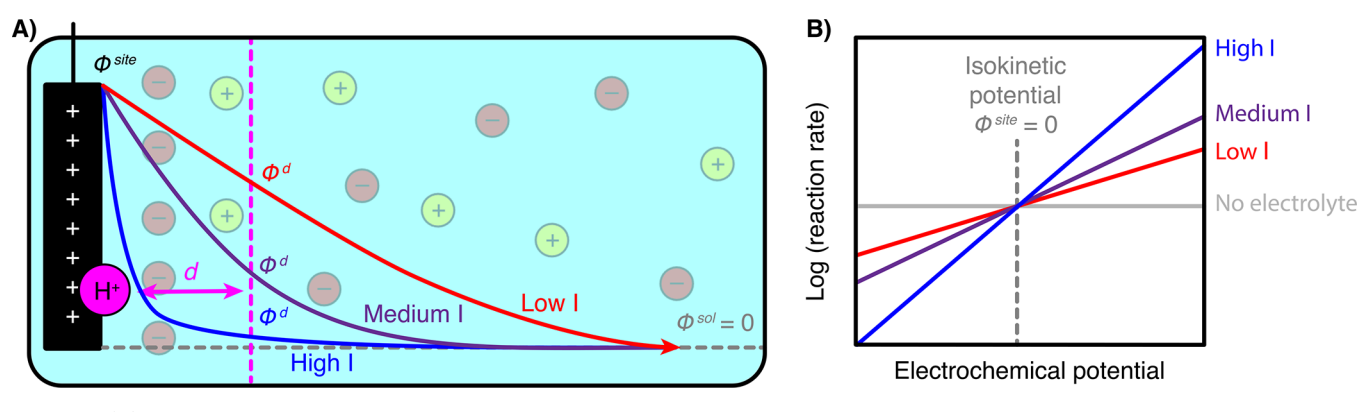


Figure 2. (A) Schematic of the electrostatic potential profile between a charged electrode and an electrolyte solution. The electrostatic potential decays quasi-exponentially from  $\phi^{\text{site}}$  at the electrode surface to  $\phi^{\text{sol}}$  in the bulk solution, taken to be zero for convenience. The decay length scale depends on ionic strength, with higher ionic strengths resulting in faster decay to the bulk solution potential. If a positively charged H+ on the electrode surface moves a distance d into solution, the electrostatic potential  $\phi^d$  depends on the ionic strength. (B) Qualitative graph of expected rate-potential scaling for electric field-induced Brønsted acid catalysis. We expect to observe a log-linear dependence of reaction rate with electrochemical potential, where larger ionic strengths result in steeper slopes. Furthermore, we expect all the rate-potential scalings to intersect at a particular electrochemical potential at which  $\phi^{\text{site}} = 0$ , denoted the isokinetic potential.

contained low site densities (estimated upper-bound active site density of 150 nM on Ti foil)<sup>24</sup> and were therefore difficult to characterize. We identified commercially available carboxylic acid-functionalized multi-walled carbon nanotubes (COOH-CNTs) with a high carboxylic acid density (~2.4 mmol/g, supplier reported), which we verified using infrared spectroscopy (Figure S5). These COOH-CNTs exist as a black powder, with each particle consisting of intertwined nanotube aggregates, as seen by scanning electron microscopy (Figure S9). However, attempts to dropcast COOH-CNTs onto electrodes resulted in agglomeration and poor dispersion, preventing us from reproducibly preparing electrodes with accurate sample masses.

To overcome this obstacle, we developed a "3D basket electrode," in which the COOH-CNT powder is encased in an electrically conductive stainless steel mesh that is sufficiently porous to allow mass transfer of reagents into the basket, yet fine enough to prevent agglomerated catalyst particles from escaping out of the basket. This design allowed for precise catalyst polarization via a potentiostat, similar to 2D electrodes, but with significant advantages for studying non-Faradaic promotion (Figure 1B). Unlike 2D electrodes with limited active site densities, the 3D basket electrodes can be loaded with much larger amounts of catalyst particles, thereby drastically increasing the total number of active sites in the reactor (estimated active site density from reactive base titrations of ~0.2 mM is ~1000-fold greater than the previously reported 2D electrodes, vide infra), 24 allowing reaction kinetics to be measured accurately across a wide range of conditions, including at low applied potentials where rates are low but undesirable side effects from leakage current are minimal. Additionally, the direct use of catalyst powders in the basket electrode reduces electrode-to-electrode variability, as the powders are withdrawn from a well-mixed batch, in contrast to 2D electrodes that often exhibit significant batchto-batch variation due to individually preparing each electrode via dropcasting from a catalyst-containing solution. 30-32 Furthermore, catalyst powders are more amenable to characterization than 2D electrodes, facilitating deeper understanding of the active site structure. We note that although basket electrodes are typically undesirable for electrocatalysis (due to large resistive losses inside the basket when passing

current), basket electrodes are well suited for studying non-Faradaic promotion, where current is minimal (ideally, zero for a purely capacitive system) and resistive losses are negligible.<sup>33</sup>

We confirmed that all the COOH-CNT powder encased in the basket reactor could be directly polarized, as inferred from kinetic and electrochemical measurements in which reaction rate and leakage current scaled linearly with catalyst mass (Figure S20). The SS mesh was selected as the basket material due to its electrical conductivity and relative inertness for Brønsted acid catalysis at the reaction conditions employed here, as we did not observe any background reactivity from the empty mesh. The reactor system was constructed with a COOH-CNT/SS basket electrode as the WE, a leakless Ag/ AgCl RE, and a Ti foil CE (Ti was also chosen as being inert for Brønsted acid catalysis under our reaction conditions)<sup>24</sup> (Figure 1C). The electrodes were inserted through a septumsealed 20 mL glass batch reactor using Ti wire connections and were controlled via a potentiostat. When immersed in a stirred electrolyte solution, the basket electrode setup allowed for simultaneous measurement and control of the applied potential on the COOH-CNT powder, while tracking the reaction kinetics. We did not observe leaching from COOH-CNTs encased in the SS basket during any experiments, likely due to the tendency of COOH-CNTs to agglomerate in solution.

To determine if applied potential in the COOH-CNT basket reactor could promote Brønsted acid catalysis, we used the liquid-phase dehydration of 1-methylcyclopentanol (MCPol) to 1-methylcyclopentene (MCPene) as a probe reaction (Figure 1A). This reaction was previously found to be highly sensitive to applied potential on 2D electrodes, with rate-potential scale factors of 70-100 mV of applied potential per 10-fold rate increase.<sup>24</sup> The reaction was performed using 100 mM MCPol and 100 mM tetrabutylammonium hexafluorophosphate (TBA PF<sub>6</sub>) in acetonitrile (MeCN), where TBA PF<sub>6</sub> was chosen as a stable, noninteracting electrolyte in accordance with previous work in our groups.<sup>2</sup>

In the absence of applied potential or electrodes, using 10 mg of COOH-CNT powder in 1 mL of reaction solution at 25 °C, only ~0.2% product yield was obtained after 2 weeks due to the low intrinsic acidity of carboxylic acids. However, when the same amount of COOH-CNT powder was placed in the basket reactor and polarized to 1.3 V vs Ag/AgCl in 10

mL of reaction solution, ~1% product yield was obtained after just 5 min of reaction time. In control experiments where no COOH—CNT catalyst was added under otherwise identical conditions, no product was detected, confirming the catalytic role of COOH—CNTs. The observed rate enhancement of approximately 100,000-fold was enabled by using the basket reactor with catalyst powders, which allowed for sufficiently high active site densities to measure a reaction rate, albeit a slow one, without any applied potential.

**Theoretical Behavior of Electric Field-Induced Brønsted Acid Promotion.** To determine if the observed rate enhancement with applied potential was due to the magnitude of the interfacial electric field, rather than alternative promotional effects (such as active site generation, specific electrolyte interactions, or Faradaic H<sup>+</sup> generation), we developed a qualitative model of electric field-induced Brønsted acid catalysis which adapts and extends derivations we previously proposed. <sup>24,34</sup> This model provides a mechanistic basis for diagnosing electric field effects using kinetic experiments.

When an electrode is charged in the presence of electrolyte, the accumulation of charge in the electrode generates an electric field between the electrode surface and the chargebalancing electrolyte ions.<sup>33</sup> At constant temperature and pressure, the electrostatic contribution to the free energy change upon moving a charge q through this electric field can be expressed in terms of an electrostatic potential function  $\phi(r)$ , where  $\phi$  is the negative integral of the electric field and r is the distance from the electrode surface.<sup>35</sup> Although the exact form of  $\phi(r)$  is not known with atomic-scale resolution, macroscopic continuum models predict a quasi-exponential decay from the electrode conductive interface  $(\phi^{\text{electrode}})$  to the bulk solution ( $\phi^{\text{sol}}$ , taken to be zero for convenience) (Figure 2A) over a characteristic length scale of angstroms to nanometers for typical solvents and electrolyte concentrations.<sup>33</sup> If we assume that the active site is situated at the electrode conductive interface, its electrostatic potential  $(\phi^{\text{site}})$ is equal to that of the electrode (i.e.,  $\phi^{\text{site}} = \phi^{\text{electrode}}$ ), though this may vary depending on the exact structure and position of the active site (which is unknown for our catalytic system).

In our qualitative model of Brønsted acid catalysis, we assume that during a catalytic cycle, a proton dissociates from the active site and traverses some distance d to its acceptor, where the electrostatic potential is  $\phi^d$  (Figure 2A). Thus, at constant temperature and pressure, the electrostatic free energy contribution of moving the positively charged proton during the deprotonation is given by

$$\Delta G_{\text{electrostatic}} = -F(\phi^{\text{site}} - \phi^d) \tag{1}$$

where F (Faraday's constant) serves as a unit conversion factor from charge to moles.<sup>24</sup> If d and the decay profile of  $\phi(\mathbf{r})$  do not vary significantly with applied potential (assumptions in our model supported by comparison with experimental rate-potential scalings, *vide infra*), then  $\phi^{\text{site}}$  is proportional to  $\phi^d$ , allowing us to set

$$\phi^d = \alpha \phi^{\text{site}} \tag{2}$$

where we define a variable  $\alpha$  ( $0 \le \alpha \le 1$ ) to serve as the proportionality constant. We can therefore express  $\Delta G_{\rm electrostatic}$  as

$$\Delta G_{\text{electrostatic}} = -F\phi^{\text{site}}(1-\alpha) \tag{3}$$

Hence, generating an electrostatic potential difference between  $\phi^{\text{site}}$  and the bulk solution can alter the deprotonation free energy  $\Delta G_a$  by

$$\Delta G_a = \Delta G_a^0 + \Delta G_{\text{electrostatic}} \tag{4}$$

where  $\Delta G_a^0$  is the deprotonation free energy in the absence of an electric field. As the acid deprotonation equilibrium constant  $K_a$  is related to the deprotonation free energy  $\Delta G_a$  by

$$K_a = e^{-\frac{\Delta G_a}{RT}} = K_a^0 e^{-\frac{\Delta G_{\text{electrostatic}}}{RT}}$$
 (5)

where R and T respectively denote the ideal gas constant and temperature, and  $K_a^0$  denotes the acid deprotonation equilibrium constant in the absence of an electric field.<sup>36</sup> Thus, altering  $\Delta G_{electrostatic}$  results in a concomitant change in  $\Delta G_{a\prime}$  and hence an exponential change in  $K_{\rm a.}$  Intuitively, a positively charged electrode surface repels the H<sup>+</sup> into solution, increasing the effective acidity of the active site and accelerating the reaction by protonating the substrate. Conversely, a negative charge buildup in the electrode near the active site attracts the H+, decreasing the effective acidity of the active site and slowing the reaction. For Brønsted acidcatalyzed reactions, the reaction rate often depends on the activity of the protonated substrate for cases when the reaction rate is limited by the acidity of the catalyst;<sup>37</sup> therefore, we expect that the reaction rate should increase linearly with  $K_a$ and thus exponentially increase with  $\phi^{\text{site}}$ . If the H<sup>+</sup> traverses the entire potential drop during deprotonation ( $\alpha \approx 0$ ), the theoretical rate-potential scaling at  $T = 25^{\circ} C$  should reach the Nernstian value of 59 mV/decade.<sup>33</sup> However, if the H<sup>+</sup> only traverses a fraction of the potential drop  $(\alpha > 0)$ , we would expect the rate to be less sensitive to potential, yielding a scaling higher than 59 mV/decade. In this case, the rate scaling depends on the value of  $\alpha$ , which in turn depends on the length scale of the electrostatic potential decay into solution. The characteristic length scale for this decay from macroscopic continuum theories is denoted as the Debye length  $\lambda_D$ , given

$$\lambda_D = \sqrt{\frac{\varepsilon_0 \varepsilon_r RT}{2F^2 I}} \tag{6}$$

where  $\varepsilon_0$  is the vacuum permittivity,  $\varepsilon_{\rm r}$  is the relative dielectric constant of the solvent (taken as 37.5 for MeCN), <sup>38</sup> and I is the ionic strength of the electrolyte, which for a simple 1:1 electrolyte is equal to the electrolyte concentration. <sup>39</sup> Since  $\lambda_{\rm D}$   $\sim I^{-1/2}$  high ionic strength shortens  $\lambda_{\rm D}$ , increasing potential sensitivity, whereas low ionic strength increases  $\lambda_{\rm D}$ , decreasing sensitivity (Figure 2A). Thus, changing ionic strength alters  $\alpha$  and therefore the rate-potential scaling.

When a "potential" (conventionally denoted E, not to be confused with electric field E) is applied to the WE relative to a RE, the measured value does not correspond to the electrostatic potential  $\phi^{\rm site}$ , but rather it reflects the difference in electron electrochemical potentials

$$E = -\frac{1}{F}(\hat{\mu}_e^{\text{site}} - \hat{\mu}_e^{RE}) \tag{7}$$

where  $\hat{\mu}_e^i$  denotes the electrochemical potential of electrons in material *i*, and *F* serves to convert *E* from units of energy/mol to energy/charge by convention.<sup>40</sup> The electron electro-

chemical potential  $\hat{\mu}_e^i$  is composed of contributions from both the electron chemical potential  $\mu_e^i$  (a property of material i) and the electrostatic potential  $\phi^i$  by

$$\hat{\mu}_e^i = \mu_e^i - F\phi^i \tag{8}$$

If we assume  $\mu_e^{\text{site}}$  to be constant with changes in applied electrochemical potential  $E^{40}$  and  $\hat{\mu}_e^{RE}$  to be constant for a particular RE/solvent combination (which is a requisite property for a stable RE),<sup>33</sup> then changes in E correspond directly to changes in  $\phi^{\text{site}}$  by

$$\phi^{\text{site}} = E + \frac{1}{F} (\mu_e^{\text{site}} - \hat{\mu}_e^{RE}) \tag{9}$$

allowing us to predict a log-linear scaling between  $K_a$  (a proxy for reaction rate) and applied potential E by

$$K_a = K_a^0 e^{\frac{(FE + \mu_e^{\text{site}} - \hat{\mu}_e^{RE})(1 - \alpha)}{RT}}$$
 (10)

Moreover, as ionic strength varies, rate-potential scaling should change, with steeper slopes at higher ionic strengths (rate is more potential-sensitive, smaller  $\alpha$ ) and shallower slopes at lower ionic strengths (rate is less potential-sensitive, larger  $\alpha$ ). In the absence of electrolyte, the rate-potential scaling should be nearly flat ( $\alpha \approx 1$ ).

Importantly, the rate-scaling lines at varying ionic strengths should all intersect at a particular electrochemical potential, denoted the "isokinetic potential" (IKP), where reaction rates are invariant to ionic strength (Figure 2B). The IKP represents the electrochemical potential at which the net charge on the electrode near the active site is zero, given by

$$IKP = -\frac{1}{F}(\mu_e^{\text{site}} - \hat{\mu}_e^{RE})$$
(11)

At the IKP,  $\phi^{\rm site}=0$  and there is no electrostatic potential drop experienced by the H<sup>+</sup> leaving the active site. This IKP allows determining  $\phi^{\rm site}$  at any applied electrochemical potential E by the equation

$$\phi^{\text{site}} = E - \text{IKP} \tag{12}$$

recasting the log-linear rate-potential scaling as

$$K_a = K_a^0 e^{\frac{F(E - IKP)(1 - \alpha)}{RT}} \tag{13}$$

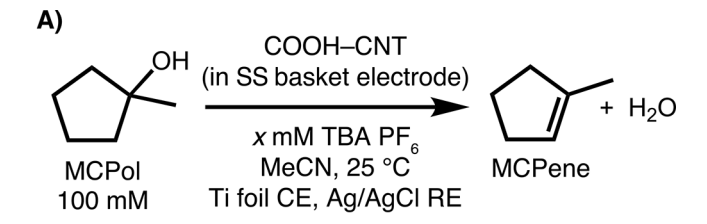
Thus, reaction rates are *promoted* when E > IKP because the electric field repels the proton from the active site, increasing acidity, and rates are demoted when E < IKP because the electric field attracts the proton to the active site, decreasing acidity; the ionic strength affects the rate-potential sensitivity by modulating  $\lambda_D$ , which changes  $\alpha$  (Figure 2B). We note that the IKP may differ from the potential of zero free charge (PZFC), which is defined as the electrochemical potential where the net free charge excess on the entire electrode is zero. At PZFC, because the local composition of an electrode can vary spatially, it is possible to have a scenario in which electrode areas near the active sites are locally charged, but other areas of the electrode are oppositely charged so that the net free charge is zero, whereas at IKP, the net free charge on electrode areas near the active sites is zero, but the free charge on other areas of the electrode away from active sites may be nonzero. One may therefore consider the IKP as an active-sitespecific PZFC, which may differ from the bulk PZFC. While

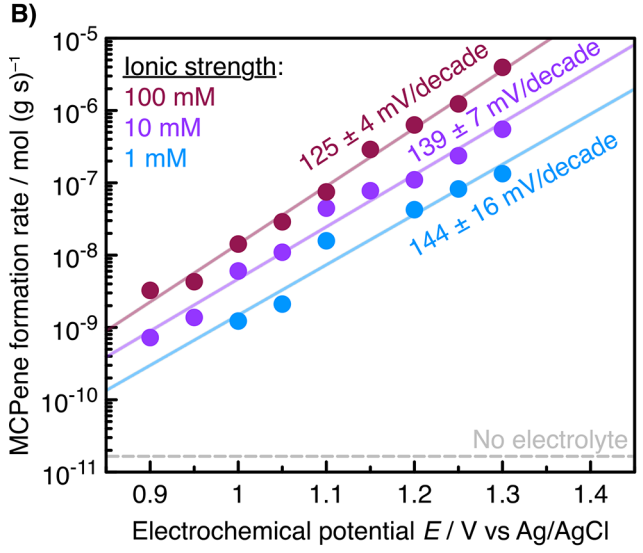
bulk PZFC can be measured through standard techniques,<sup>41</sup> determining IKP requires active-site-specific kinetic measurements. Similarly, IKP does not necessarily coincide with the open circuit potential (OCP), which reflects the equilibrium potential of the system in the absence of an applied bias and may be influenced by redox-active species in solution.<sup>33</sup>

The predicted outcomes of our model offer clear experimental diagnostic signatures that distinguish electric field-induced catalysis from Faradaic H+ generation as potential-based promotion mechanisms. Both mechanisms exhibit log-linear rate-potential scalings at high potentials, but only electric field-induced catalysis should display an IKP and is expected to show rate demotion below IKP. Previous studies have only observed the log-linear rate-potential scalings at high positive potentials due to the low density of active sites on 2D electrode surfaces, complicating the convoluting effects of interfacial electric fields and Faradaic H<sup>+</sup> generation. By using basket electrodes with drastically higher active site densities than 2D electrodes, we hypothesized that our COOH-CNT/SS basket electrode system would allow us to observe the full spectrum of predicted behavior and confirm whether electric field-induced rate promotion governs the observed catalytic activity. As such, we sought to perform detailed kinetics studies to determine if the outcomes aligned with our model predictions.

Kinetics and Mechanism of Electric Field-Promoted Alcohol Dehydration. To validate our model predictions of log-linear rate potential scaling and identify the IKP, we conducted kinetics measurements on the liquid-phase dehydration of MCPol to MCPene catalyzed by COOH-CNT as a Brønsted acid catalyst at varying electrochemical potentials and ionic strengths. We performed batch reactions using the COOH-CNT/SS basket electrode (Figure 1C) with 100 mM MCPol in varying concentrations of TBA PF<sub>6</sub> electrolyte in MeCN at 25 °C, using a leakless Ag/AgCl RE and a Ti foil CE (Figure 3A). All electrochemical potentials are reported with respect to this RE unless otherwise specified. We quantified MCPol and MCPene using <sup>1</sup>H NMR spectroscopy of the reaction solution, using TBA PF<sub>6</sub> as an internal standard (Figure S30), with peak areas corrected for ionic strengthdependent relaxation delay times (Figure S32).<sup>24</sup>

Control experiments confirmed that COOH-CNT catalyzed the reaction heterogeneously. Product yields corresponded to initial rates as product formation was linear with time up to ~10% conversion, indicating that initial rates were unaffected by catalyst deactivation or changes in water content (Figure S15). At higher conversions ( $\sim$ 20%), a minor amount of the anti-Zaitsev product, methylenecyclopentane, was observed, but MCPene remained the dominant product (>99% selectivity), justifying the use of MCPene yield to determine reaction rates. No product was detected in the absence of COOH-CNT, ruling out contributions from other materials in the system (i.e., background reactivity from the SS basket WE, Ag/AgCl RE, Ti foil CE, PTFE stir bar, or glass reaction vial). A hot filtration test confirmed that leached species did not contribute to reactivity, and removing the applied polarization stopped the reaction, indicating that the promotional effect does not result from irreversible structural changes to the catalyst under applied polarization (Figure \$16). Adsorption studies showed negligible MCPene binding to COOH-CNT (Figure S29), and RE calibration with decamethylferrocene confirmed that the RE potential remained





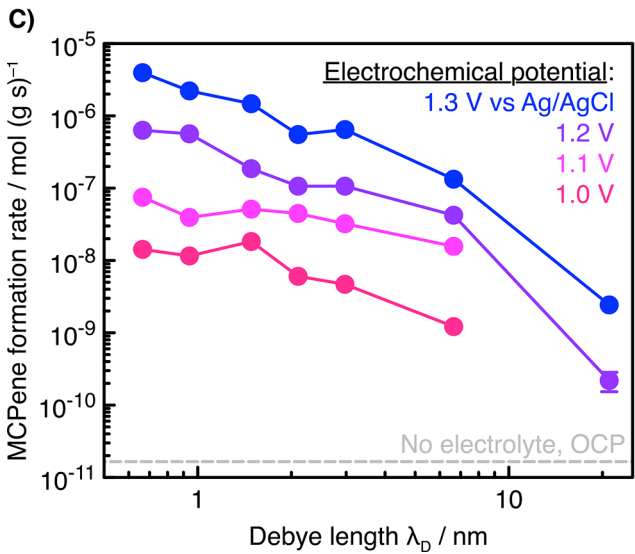


Figure 3. (A) Scheme of alcohol dehydration used as a probe reaction for this study. (B) Log–linear rate dependence of MCPene formation on electrochemical potential ( $iR_{\rm u}$  corrected in situ using current interrupt) at a range of ionic strengths. Propagated uncertainties in rate measurements are shown in y-axis error bars or are smaller than the data point height. Standard deviations of electrochemical potential are smaller than the data point width. The dashed gray line corresponds to the reaction rate without added electrolyte or applied electrochemical potential. (C) Dependence of MCPene formation rate on Debye length  $\lambda_{\rm D}$  (changed by altering ionic strength) at a range of electrochemical potentials. Error bar conventions align with those in Figure B.

stable with changes in reactant concentration and ionic strength (Section S5).

With these controls in place, we measured reaction rates as a function of electrochemical potential and found a log—linear rate dependence on applied potential, consistent with our

model and prior work on potential-promoted alcohol dehydration (Figure 3B). At 100 mM ionic strength, we obtained a rate-potential scaling of  $125 \pm 4 \text{ mV/decade}$ , which is larger than the expected Nernstian scaling of 59 mV/decade. This discrepancy, also observed in previous studies (ratepotential scalings ranging from 70-100 mV/decade with different catalysts),<sup>24</sup> could arise from several factors: (1) the H<sup>+</sup> does not traverse the full electrostatic potential drop from the WE to the bulk solution upon proton transfer to the substrate, (2) disordered or weakly conductive carbon fragments act as dielectric layers between the H+ bound to the acid site and the bulk conductive carbon, introducing an electrostatic potential drop between the WE and the acid site, or (3) the positively charged H<sup>+</sup> leaving the WE is counterbalanced by an approaching TBA+ cation during deprotonation, decreasing the net charge that traverses the electrostatic potential drop. Given that our catalyst consists of multi-walled carbon nanotubes, the exact positioning of active sites relative to the overall electrode-solution potential drop remains unclear, and minor carbonaceous impurities may also contribute to reactivity. Further investigations are needed to distinguish between these possibilities.

To probe ionic strength effects, we measured reaction rates at electrolyte concentrations ranging from 1 mM to 100 mM (Figure 3B). As predicted, reaction rates increased with ionic strength, but surprisingly, the rate-potential scalings were within experimental error across all concentrations (125-144 mV/decade). This suggested that the IKP, where rate is independent of ionic strength, lies outside the tested potential range. Lowering the potential further was impractical with these reaction conditions, as at 0.9 V the reaction required 3 days to achieve measurable product yield (~0.1%). We note that although the rate at 0.9 V is quite slow, it is still promoted ~50-fold relative to the rate obtained without any electrodes and applied polarization, which required several weeks to obtain measurable product yield (Figure S13). We found it surprising that the rate scaling at 1 mM ionic strength was so close to that at 100 mM ionic strength, given that the 1 mM ionic strength is so dilute that there are more COOH groups on the COOH-CNTs than electrolyte molecules in solution.

To further investigate the role of ionic strength, we extended measurements to 0.1 mM electrolyte concentration. At this low ionic strength, the reaction remained promoted compared to the electrolyte-free case, but rates were significantly lower than at 1 mM (Figure S12). Unfortunately, at such low ionic strengths, the potentiostat was not able to stably maintain the set point potential while compensating for solution resistance, which led to large oscillations in electrochemical potential. Consequently, reliable log—linear rate-potential scaling at such low ionic strength could not be obtained, but the results suggest that the expected rate scaling attenuation occurs below 1 mM. Notably, without added electrolyte, no product was detected at 1.3 V, confirming that trace ionic impurities were insufficient to induce rate promotion.

By calculating the Debye length  $\lambda_{\rm D}$  for each ionic strength, we examined the rate sensitivity to  $\lambda_{\rm D}$  at constant electrochemical potential (Figure 3C). In our model, the H<sup>+</sup> moves a distance d from the WE into the bulk solution during the catalytic cycle to protonate MCPol (Figure 2A); this likely occurs from first protonating MCPol coordinated to the active site H<sup>+</sup>, after which the protonated MCPol travels some distance into the bulk solution where it undergoes dehydration (Scheme 1). If  $d \gg \lambda_{D}$ , then the H<sup>+</sup> experiences the full

Scheme 1. Proposed Mechanism of MCPol Dehydration Catalyzed by  $COOH-CNT^a$ 

Ist order kinetics

MARI

HO

H

For 1st order kinetics:

$$TOF \approx kK_1K_2a_{MCPol}$$
 $K_2(E)$ 
 $K_3(E)$ 
 $K_3(E)$ 
 $K_3(E)$ 
 $K_3(E)$ 
 $K_2(E)$ 
 $K_2(E)$ 

"This proposed  $E_1$ -type mechanism involves quasi-equilibrated reactant adsorption and protonation, followed by rate-determining carbocation formation, then quasi-equilibrated deprotonation and product desorption. The asterisk [\*] represents a Brønsted acidic active site on the WE. Presence of an applied electric field E alters the protonation equilibrium constant  $K_2$  due to (de)stabilizing the charge separation that occurs during active site deprotonation. In the first-order rate regime in which the MARI is the non-coordinated site, the TOF rate expression depends linearly on  $K_2$ , thus electric field application can alter reaction rate through modulating  $K_2$ . Pink arrows represent an arrow-pushing mechanism to aid in following the mechanistic cycle.

electrostatic potential drop during deprotonation, so  $\alpha\approx 0$  and the rate becomes insensitive to  $\lambda_{\rm D}$ . Conversely, if  $d\gg\lambda_{\rm D}$ , then the H<sup>+</sup> only traverses part of the electrostatic potential drop ( $\alpha>0$ ), leading to a decrease in rate with increasing  $\lambda_{\rm D}$ . Our experimental results agreed qualitatively with our model, showing that the reaction rate was relatively insensitive (within the same order of magnitude) to  $\lambda_{\rm D}$  for  $\lambda_{\rm D}<\sim 5$  nm, but that it decreased more sharply for  $\lambda_{\rm D}>\sim 5$  nm. This observation applied to our qualitative model suggests that d is on the order of 5 nm under these ideal assumptions, although we note that deviations from ideality of interfacial ionic composition may complicate this analysis.

In line with our prior study, we invoke that MCPol dehydration follows an  $E_1$  pathway typical for tertiary alcohols (Scheme 1), which consists of quasi-equilibrated MCPol adsorption and protonation followed by carbocation formation as the rate-determining step (RDS).<sup>24</sup> Our model predicts that electric fields enhance the protonation equilibrium constant  $K_2$ , leading to an increased fraction of protonated MCPol species and thus higher turnover frequency (TOF) values. Indeed, the derived rate law for this mechanism contains a first-order regime at low MCPol activities, where the most abundant reactive intermediate (MARI) is the non-coordinated site. At higher MCPol activities, the rate law transitions

to a zero-order regime where the MARI becomes MCPol coordinated to the site (Section S7). We found that the rate is first order in MCPol concentration for our reaction conditions, indicating that the MARI is the non-coordinated site (Figure S17). Nevertheless, the rate expression for the first-order regime depends linearly on  $K_2$ , which determines the pre-RDS equilibrium. Intuitively, an increase in  $K_2$  corresponds to increasing the activity of the protonated intermediate vs unbound MCPol (Scheme 1); this provides the mechanistic basis for the electric field-induced rate promotion.

Although the configuration of applying potential to electrodes for electric field-promoted catalysis is similar to that used in electrocatalysis, the two frameworks are conceptually distinct. In electrocatalysis, the formation of each product molecule requires a fixed number of electrons transferred from current flow, and efficiency is characterized by the selectivity of current-passed electrons to desired product (termed Faradaic Efficiency).<sup>33</sup> Contrastingly, in electric field-induced catalysis, the promotional effect of applied potential should be non-Faradaic and therefore orthogonal to the current. Ideally, there should be no charge passed if the system acts purely capacitively, but in practice the presence of redox-active components or impurities generally leads to a small leakage current. To distinguish between thermocatalytic and electrocatalytic promotion, we define an analogous "pseudo-Faradaic Efficiency" (pFE) as the ratio of additional product formed (relative to the rate at OCP) per charge passed.<sup>24</sup> While electrocatalysis has a maximum pFE of 100%, thermocatalysis can exhibit arbitrarily large pFE values if leakage currents are small. Hence, observation of pFE exceeding 100% for potential-promoted catalysis is sufficient to demonstrate that rate promotion is thermocatalytic.

Although the basket electrode was designed to act capacitively, we observed a leakage current that increased with polarization and ionic strength. Upon polarization, a transient capacitive charging current rapidly decayed to a steady-state value, which likely resulted from trace redox-active impurities (such as water splitting) or partial carbon oxidation at higher potentials (Figure S19). Currents averaged over the first 5 min ranged from 1-200  $\mu$ A/mg, depending on ionic strength and polarization (Figure S18). Despite this result, pFE values exceeded 100% in most cases, reaching up to 300%, demonstrating that the promotion was non-Faradaic. However, this alone did not confirm that electric fields, not Faradaic H<sup>+</sup> generation, were responsible for rate enhancement. If electrochemically generated protons catalyzed multiple turnovers, the overall reaction would still be non-Faradaic with pFE values potentially greater than 100%, but the mechanism would be different. To distinguish between these two mechanisms, we sought to quantify and probe the behavior of the promoted active sites.

Quantification of Kinetically Relevant Active Sites on Carbon Nanotube Catalysts. To better understand the nature of active sites and distinguish electric field-induced promotion from other potential-promoted mechanisms, we utilized catalyst base titrations to count acidic active sites. This technique, commonly used in heterogeneous acid catalysis but previously unexplored in potential-promoted Brønsted acid catalysis, involves titrating the catalyst with a known quantity of base to selectively neutralize acid sites, thereby rendering them catalytically inactive. <sup>42</sup> Ideally, this deactivation results in a linear decrease in reaction rate with increasing base addition until the rate reaches zero, after which further base addition

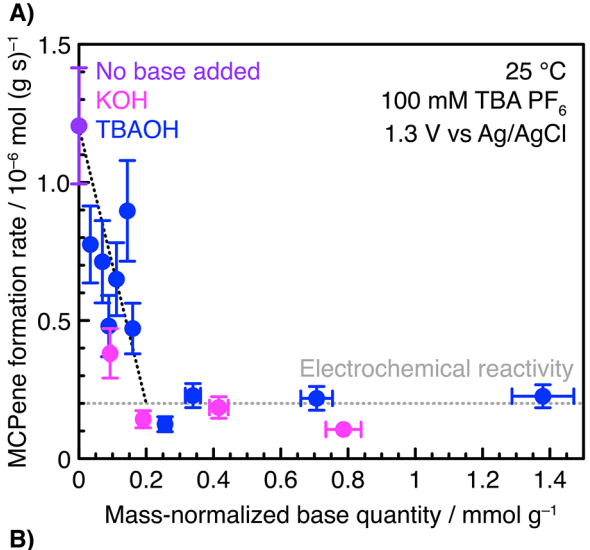
has no effect. The base quantity required to eliminate catalytic activity corresponds to the number of kinetically relevant acid sites. Previous studies on potential-promoted catalysis have estimated active site densities using geometric arguments or assuming equal activity for all added active sites, highlighting the need for a direct quantification approach.<sup>24</sup>

To measure the kinetically relevant active site density, we performed base titrations on COOH-CNT samples by soaking a known mass of COOH-CNTs in a methanol (MeOH) solution containing known, substoichiometric amounts of potassium hydroxide (KOH) overnight, followed by centrifugation/decantation and drying under vacuum. We expected the KOH to react with surface COOH groups to form potassium carboxylates and water, as verified by infrared spectroscopy, which showed decreases in C=O intensities (from COOH) and increases in COO- intensities (from potassium carboxylate species) with increasing KOH loading (Figure S6). Furthermore, we expected that the added KOH would selectively titrate the catalytically active COOH groups first as the catalytically active COOH groups should be the most acidic. The dried samples were then used as catalysts in the basket electrode at 1.3 V with 100 mM ionic strength at 25 °C.

As expected, the reaction rate initially decreased with increasing KOH loading; however, the rate surprisingly plateaued above ~0.2 mmol/g of KOH, where further addition of KOH did not further decrease the rate (Figure 4A). This behavior was not unique to KOH, as samples titrated with tetrabutylammonium hydroxide (TBAOH) exhibited the same plateau. We hypothesize that this residual activity stems from electrochemical reactivity via Faradaic processes, including transient H<sup>+</sup> generation, which would not be neutralized by a pre-reaction base titration. Although exploring this further is the subject of future work, regardless of the origin of this plateau region, the comparison of the relative rates indicates that  $\sim 0.2$  mmol/g of active sites account for >85% of the reactivity. Given that the total COOH concentration from supplier data is  $\sim$ 2.4 mmol/g, this suggests that only  $\sim$ 8% of the COOH sites participate in catalysis. Although we cannot conclusively explain why only a subset of COOH groups are catalytically active, we expect that differences in the local chemical structure surrounding the COOH groups and positioning within the carbon nanotubes lead to variations in acidity and field sensitivity (see Section S3.4).

Although some electrochemical background reactivity may be present, the dominant rate contribution from titratable acidic surface sites (>85% of observed reactivity at 1.3 V and 100 mM ionic strength) demonstrates that the rate promotion is primarily thermocatalytic and not driven by electrochemically generated species, such as H<sup>+</sup> formed from leakage current. We expect the electrochemical rate contribution to be smaller at lower polarizations as the current is zero at OCP and therefore no Faradaic H<sup>+</sup> can be generated. The electrochemical rate contribution is also smaller at lower ionic strengths, as COOH-CNT titrated with ~1.4 mmol/g of TBAOH (in the plateau region) does not yield detectable product at 1.3 V with 0.1 mM ionic strength.

With the ability to count active sites under polarization, we examined whether certain sites were more responsive to electric field-induced promotion. To test this hypothesis, we compared our measured active site densities under polarized and unpolarized conditions (which we could approximate by measuring reaction rates in the absence of added electrolyte).



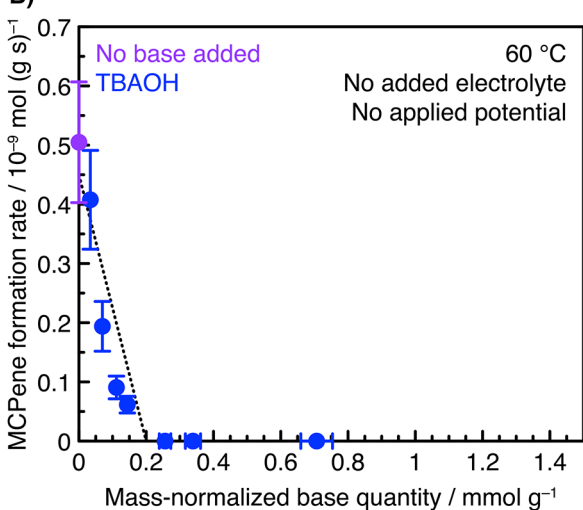


Figure 4. Base titrations of COOH-CNTs showing an active site density of ~0.2 mmol/g. Error bars are propagated from experimental uncertainties. Dashed lines are shown to guide the eye. Purple, blue, and pink colors respectively denote no base added, KOH titration, and TBAOH titration. (A) Rate data were collected using the basket electrode at 1.3 V with 100 mM ionic strength at 25 °C. The gray dashed line indicates the rate plateau with base loading, which we tentatively attribute to electrochemical background reactivity. (B) Rate data were collected with free COOH-CNT powder without added electrolyte at 60 °C in the absence of any other electrodes or polarization.

Unfortunately, the low reaction rate at 25 °C made this comparison unfeasible, as these conditions require a week of reaction time to achieve ~0.1% yield. To circumvent this issue, we increased the reaction temperature to 60 °C, which resulted in a ~70-fold rate increase, enabling practical rate measurements. Under electrolyte-free conditions at 60 °C, base titrations revealed the same active site density (~0.2 mmol/ g) as the polarized case, but in contrast to the polarized system, the reaction rate was fully suppressed beyond this loading (Figure 4B). This suggests that there are  $\sim 0.2$  mmol/g of active sites on COOH-CNT that dominate the catalytic activity, and these active sites are all promoted approximately equally under polarization. Furthermore, the lack of a nonzero plateau region in the electrolyte-free case is consistent with our assignment of the nonzero plateau region at 1.3 V to

electrochemical artifacts, as no current was passed in the electrolyte-free case and thus the rate was eliminated by base titration.

Given prior reports that the catalytic activity of carbon nanotubes can originate from metal impurities rather than the nanotube structure itself, 43 we sought to verify that the catalytic activity of COOH–CNT was not due to metal impurities. Thermogravimetric analysis (TGA) decomposition of COOH–CNT revealed that ~3.7 wt % of material remained upon heating to 800 °C under air, which suggested the presence of metal impurities as these conditions should oxidize/volatilize all organic matter (Figure S7). We attempted to purify the COOH–CNTs by washing with hydrochloric acid, a treatment known to reduce metal impurity content, but we were unable to remove the inorganic impurities below ~1.5 wt % with this treatment (Figure S8).

To address this issue, we performed energy dispersive X-ray (EDX) mapping to identify the metal impurities present in COOH-CNT, which revealed the possible presence of Al, Ca, Cl, Co, Fe, and Si in addition to the expected H, C, and O (due to low peak intensities of the metal impurities from EDX, clear assignment of the peaks to elements was not always possible, so our list includes all possible elements that could be reasonably fitted to the EDX spectrum) (Section S2.4). For Al, Ca, Co, Fe, and Si, we tested catalytic activity of their oxide forms (to mimic a potential structure of these impurities on the nanotubes)45 using 20 mg of oxide in 2 mL of electrolyte-free reaction solution at 80 °C for 3 days; none of these yielded any detectable product. We additionally performed elemental analysis on COOH-CNT to quantify the elements present in our list and determine if any of them could be responsible for the catalytic activity (Table S3); gratifyingly, all of the element loadings were significantly less than 0.2 mmol/g, indicating that they could not be responsible for all of the catalytic activity as the measured active site density was ~0.2 mmol/g. Collectively, these control experiments establish that the catalytic activity of COOH-CNT originates from acidic surface groups rather than metal contaminants. Furthermore, the ability to quantify active sites under polarization and the consistent rate suppression beyond ~0.2 mmol/g of titrant demonstrate that all active sites experience uniform rate enhancement under applied potential. This confirms that electric field effects, rather than electrochemical H<sup>+</sup> generation or site heterogeneity, drive the observed rate promotion.

Tunable Rate Promotion/Demotion and Crossover at **Isokinetic Potential.** Encouraged by the easily measurable reaction rates at 60 °C using unpolarized COOH-CNTs, we hypothesized that we could measure rate demotion by polarizing negative of IKP in addition to rate promotion by polarizing positive of IKP, allowing us to identify the IKP as the unique intersection point of rate-potential scaling lines with varying ionic strength. Additionally, since current is passed whenever the system is polarized away from OCP, a mechanism based on electrochemically generated species would predict that any polarization - whether positive or negative relative to OCP - should always result in a rate increase. Therefore, demonstrating rate demotion below OCP (which need not equal the IKP) would further confirm that the observed potential-dependent kinetics arise from an electric field-induced mechanism rather than electrochemically generated species.

Using the COOH-CNT/SS basket reactor at 60 °C, we measured the MCPene formation rate at 100 mM ionic

ı

strength with varying electrochemical potential, yielding an expected log-linear dependence with a rate scaling of  $141 \pm 6$  mV/decade (Figure 5). This increase in rate scaling at higher

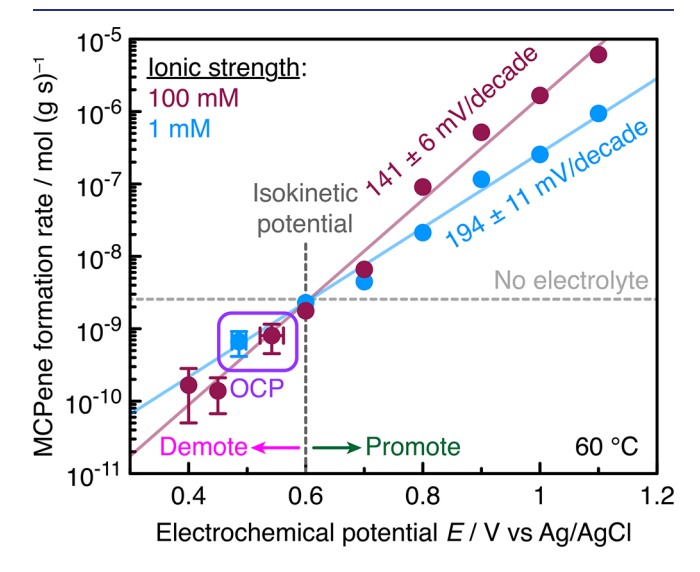


Figure 5. Tunable log—linear promotion/demotion of MCPene formation rate catalyzed by COOH—CNT with electrochemical potential ( $iR_{\rm u}$  corrected in situ using current interrupt above 0.8 V, at which  $iR_{\rm u} > 10$  mV) at 1 mM and 100 mM ionic strength at 60 °C. Propagated uncertainties in rate measurements are shown in y-axis error bars or are smaller than the data point height. Standard deviations of electrochemical potential are shown as x-axis error bars or are smaller than the data point width. Larger x-axis error bars are shown for OCP reactions due to the measured OCP drifting during the reaction. The dashed gray line corresponds to the reaction rate without added electrolyte or applied electrochemical potential. The isokinetic potential occurs at the intersection of the rate scaling lines.

temperatures (compared to 125  $\pm$  4 mV/decade at 25 °C) is consistent with the expected equilibrium constant temperature dependence and has also been observed previously with other catalysts (Section S8).<sup>24</sup> We also measured the reaction rate at OCP, where the COOH-CNT was in the basket reactor but without any applied polarization; instead, we used the basket reactor to measure OCP during the reaction. The rate obtained at OCP aligned with the rate scaling trend established by polarized data, supporting the conclusion that the reaction follows the same mechanism at OCP. The OCP exhibited a drift of ~80 mV over the course of the day-long reaction, which we attribute to unidentified redox-active impurities in the reaction solution, but this drift remained small compared to the large range of electrochemical potentials examined in this study (Figure S22). Importantly, polarizing negative of OCP resulted in rate demotion that also fell on the ratepotential scaling line, demonstrating that the rate alteration mechanism is not due to electrochemically generated species. Similar to the 25 °C rate data, the leakage currents increased with polarization and featured pFE values as high as 1400%, further supporting that the mechanism for rate promotion is non-Faradaic (Figure S23).

Given the extended range of electrochemical potentials with measurable reaction rates at 60  $^{\circ}$ C (0.4 to 1.1 V), we sought to experimentally locate the theorized IKP. To probe this, we collected rate data with varying electrochemical potential at 1 mM ionic strength, as this was the lowest ionic strength (and therefore largest expected rate scaling difference) we could use

to reliably polarize with in situ iR<sub>u</sub> correction. The 1 mM ionic strength scaling of 194  $\pm$  11 mV/decade is larger than the 100 mM ionic strength scaling of 141 ± 6 mV/decade, consistent with what we observe at 25 °C. The two distinct rate scaling lines intersected at ~0.6 V, which coincided with the rate obtained in the absence of both polarization and added electrolyte, measured with free COOH-CNT powder in solution and no external electrodes (Figure 5). This behavior is consistent with the IKP concept, wherein the electrostatic potential at the active site equals the bulk solution potential, rendering the rate independent of ionic strength. An IKP of ~0.6 V is also consistent with the rate data obtained at 25 °C, in which extrapolated best-fit lines for the rate-potential scalings intersect the rate obtained without electrolyte and polarization between 0.55-0.70 V (Figure S13). The IKP location also explains why the OCP rates at 1 mM and 100 mM ionic strength are lower than the electrolyte-free case, even though ostensibly adding electrolyte should increase the rate by stabilizing the charge-separated protonated intermediate; since OCP (determined by trace unidentified redox processes) lies below the IKP, adding electrolyte generates an interfacial electric field which attracts the proton to the active site, thus lowering effective acidity and demoting the rate. Altogether, the tunable rate promotion/demotion and identification of an IKP demonstrate that the potentialdependent rate alteration proceeds via an electric field-induced mechanism, consistent with the expectations of our model. We note that the observed reaction rate at IKP is specific to MCPol and may change with varying substituents and functionalization. However, the electrostatic promotion mechanism predicts a consistent rate-potential scaling across substrates.

The ability to measure unpolarized rates at 60 °C also enabled additional control experiments that were impractical at 25 °C due to slow reaction kinetics. A key consideration was ensuring that the measured rates reflect intrinsic kinetics rather than diffusion limitations. If external mass transport were limiting, the reaction rate would be independent of polarization, which is inconsistent with our data. In the absence of added electrolyte and applied polarization to eliminate electric field effects, reaction rates with COOH-CNT in the basket electrode match those obtained with free COOH-CNT powder, demonstrating that the basket electrode does not create interparticle internal diffusion limitations (Figure S27). Assessing intraparticle diffusion limitations was more challenging due to the lack of well-defined tunable active sites, which precluded the standard approach of altering site density or particle size. However, we can use the rate scaling to argue that our rates are not internally diffusion-limited. At the lowest polarization of 0.4 V, we measured a ~0.02% product yield over the course of  $\sim 3$  days. The slow rate under these conditions suggests that the rate is not internally diffusionlimited at these low electrochemical potentials, which is supported by Thiele modulus calculations which estimate a first-order reaction effectiveness factor of >0.999 (Section S6.3). If the reaction were to become internally diffusionlimited at higher electrochemical potentials, the first-order reaction effectiveness factor would change such that the measured rate would depend on the square root of the firstorder rate constant. Since applied polarization alters the firstorder rate constant through a log-linear manner, the ratepotential scaling slope in the internally diffusion-limited region should be 1/2 of the rate scaling slope in the kinetically

controlled region. Since we do not observe this change in the rate-potential scaling slope from  $\sim 125$  mV/decade to  $\sim 250$  mV/decade and instead observe a constant log-linear rate-potential scaling over the  $\sim 5$  orders of magnitude of measured reaction rates, we conclude that our rate data reflect intrinsic kinetics and are free of diffusion limitations.

#### CONCLUSION

In this study, we investigated the electric field-induced promotion of alcohol dehydration catalyzed by Brønsted acid sites on COOH-CNTs polarized in a basket electrode configuration. This setup enabled direct polarization of catalyst powders to achieve high active site densities, overcoming the limitations imposed by previously used 2D electrodes. Using an electrostatics-based model of electric field-induced Brønsted acid promotion, we predicted a log-linear scaling between rate and electrochemical potential, attenuated scaling at low ionic strengths, and the existence of an isokinetic potential at which the reaction rate becomes independent of ionic strength. By varying electrochemical potential at a range of ionic strengths, we validated our model's predictions of the rate promotion dependency on ionic strength. Furthermore, we experimentally located the isokinetic potential at ~0.6 V vs Ag/AgCl, evidenced by a common intersection point of rate scaling lines at different ionic strengths at 60 °C. Base titration experiments to quantify active sites yielded a site count of ~0.2 mmol/g which was independent of polarization, suggesting that the active sites are uniformly polarized with applied potential for our system.

Our mechanistic study holistically demonstrates that the observed potential-based rate alteration arises from an interfacial electric field that changes the acidity of the active site through (de)stabilizing the positively charged acidic proton, in accordance with our electrostatics-based model. In particular, our demonstration of rate demotion, identification of isokinetic potential, and active site quantification experiments support this mechanism of electric field-induced promotion over a mechanism based on electrochemically generated species from leakage current. By linking molecular-scale electric field interactions with reactor-scale design, this study sets the stage for electrostatic promotion strategies in heterogeneous catalysis under mild conditions.

## ASSOCIATED CONTENT

## **Supporting Information**

The Supporting Information is available free of charge at https://pubs.acs.org/doi/10.1021/jacs.5c05891.

Raw data, design files for 3D-printed vial holder, experimental methods video (ZIP)

Materials and experimental methods, full characterization and experimental data, supplementary discussions (PDF)

#### AUTHOR INFORMATION

# **Corresponding Authors**

Yuriy Román-Leshkov — Department of Chemical Engineering, Massachusetts Institute of Technology, Cambridge, Massachusetts 02139, United States; orcid.org/0000-0002-0025-4233; Email: yroman@mit.edu

Mircea Dincă — Department of Chemistry, Massachusetts Institute of Technology, Cambridge, Massachusetts 02139, United States; orcid.org/0000-0002-1262-1264; Email: mdinca@mit.edu

Yogesh Surendranath — Department of Chemistry, Massachusetts Institute of Technology, Cambridge, Massachusetts 02139, United States; oorcid.org/0000-0003-1016-3420; Email: yogi@mit.edu

### **Authors**

- Bhavish Dinakar Department of Chemical Engineering, Massachusetts Institute of Technology, Cambridge, Massachusetts 02139, United States; orcid.org/0000-0002-7611-101X
- Karl S. Westendorff Department of Chemical Engineering, Massachusetts Institute of Technology, Cambridge, Massachusetts 02139, United States
- Juan F. Torres Department of Chemistry, Massachusetts Institute of Technology, Cambridge, Massachusetts 02139, United States
- Mostapha Dakhchoune Department of Chemical Engineering, Massachusetts Institute of Technology, Cambridge, Massachusetts 02139, United States
- Katelyn Groenhout Department of Chemical Engineering, Massachusetts Institute of Technology, Cambridge, Massachusetts 02139, United States
- Nathan Ewell Department of Chemical Engineering, Massachusetts Institute of Technology, Cambridge, Massachusetts 02139, United States; orcid.org/0009-0006-4718-9762

Complete contact information is available at: https://pubs.acs.org/10.1021/jacs.5c05891

## Notes

The authors declare no competing financial interest.

## ACKNOWLEDGMENTS

This work was supported by the Department of Energy, Office of Basic Energy Sciences, where work in the Román Lab was supported under Award DE-SC0016214 and work in the Dincă Lab was supported under Award DE-SC0023288. B.D. and K.S.W. were supported by the National Science Foundation Graduate Research Fellowship Program (GRFP) under grant number 2141064. M.D. (Mostapha Dakhchoune) was supported by the Schmidt Science Fellowship. Nuclear magnetic resonance spectroscopy was performed at the MIT DCIF via the use of its shared user facilities. Scanning electron microscopy was performed through the use of MIT.nano's facilities. We thank Prof. Zachary Smith's group for use of their thermogravimetric analysis instrument. We thank Alexander Quinn, Trent A. Weiss, and Nicholas J. Matteucci for assistance in procuring basket mesh materials. We thank Blake A. Johnson, Griffin S. Drake, and Matthew S. Webber for helpful discussions.

#### REFERENCES

- (1) Friend, C. M.; Xu, B. Heterogeneous Catalysis: A Central Science for a Sustainable Future. *Acc. Chem. Res.* **2017**, *50* (3), 517–521.
- (2) Fried, S. D.; Boxer, S. G. Electric Fields and Enzyme Catalysis. *Annu. Rev. Biochem.* **2017**, *86* (1), 387–415.
- (3) Fried, S. D.; Bagchi, S.; Boxer, S. G. Extreme electric fields power catalysis in the active site of ketosteroid isomerase. *Science* **2014**, 346 (6216), 1510–1514.

- (4) Boxer, S. G. Stark Realities. J. Phys. Chem. B 2009, 113 (10), 2972-2983.
- (5) Dubey, K. D.; Stuyver, T.; Shaik, S. Local Electric Fields: From Enzyme Catalysis to Synthetic Catalyst Design. *J. Phys. Chem. B* **2022**, 126 (49), 10285–10294.
- (6) Che, F.; Gray, J. T.; Ha, S.; Kruse, N.; Scott, S. L.; Mcewen, J.-S. Elucidating the Roles of Electric Fields in Catalysis: A Perspective. *ACS Catal.* **2018**, *8* (6), 5153–5174.
- (7) Shaik, S.; Danovich, D.; Joy, J.; Wang, Z.; Stuyver, T. Electric-field mediated chemistry: Uncovering and exploiting the potential of (oriented) electric fields to exert chemical catalysis and reaction control. *J. Am. Chem. Soc.* **2020**, *142* (29), 12551–12562.
- (8) Shaik, S.; Mandal, D.; Ramanan, R. Oriented electric fields as future smart reagents in chemistry. *Nat. Chem.* **2016**, 8 (12), 1091–1098
- (9) Léonard, N. G.; Dhaoui, R.; Chantarojsiri, T.; Yang, J. Y. Electric Fields in Catalysis: From Enzymes to Molecular Catalysts. *ACS Catal.* **2021**, *11* (17), 10923–10932.
- (10) Aragonès, A. C.; Haworth, N. L.; Darwish, N.; Ciampi, S.; Mannix, E. J.; Wallace, G. G.; Diez-Perez, I.; Coote, M. L. Electrostatic catalysis of a Diels-Alder reaction. *Nature* **2016**, *531* (7592), 88–91.
- (11) Lv, J.; Sun, R.; Yang, Q.; Gan, P.; Yu, S.; Tan, Z. Research on Electric Field—Induced Catalysis Using Single—Molecule Electrical Measurement. *Molecules* **2023**, 28 (13), 4968.
- (12) Huang, X.; Tang, C.; Li, J.; Chen, L.-C.; Zheng, J.; Zhang, P.; Le, J.; Li, R.; Li, X.; Liu, J.; et al. Electric field—induced selective catalysis of single-molecule reaction. *Sci. Adv.* **2019**, 5 (6), No. eaaw3072.
- (13) Aitken, H. M.; Coote, M. L. Can electrostatic catalysis of Diels—Alder reactions be harnessed with pH-switchable charged functional groups? *Phys. Chem. Chem. Phys.* **2018**, 20 (16), 10671—10676.
- (14) Klinska, M.; Smith, L. M.; Gryn'ova, G.; Banwell, M. G.; Coote, M. L. Experimental demonstration of pH-dependent electrostatic catalysis of radical reactions. *Chem. Sci.* **2015**, *6* (10), 5623–5627.
- (15) Blyth, M. T.; Coote, M. L. A PH-switchable electrostatic catalyst for the Diels—Alder reaction: Progress toward synthetically viable electrostatic catalysis. *J. Org. Chem.* **2019**, *84* (3), 1517–1522.
- (16) Kang, K.; Fuller, J.; Reath, A. H.; Ziller, J. W.; Alexandrova, A. N.; Yang, J. Y. Installation of internal electric fields by non-redox active cations in transition metal complexes. *Chem. Sci.* **2019**, *10* (43), 10135–10142.
- (17) Meir, R.; Chen, H.; Lai, W.; Shaik, S. Oriented electric fields accelerate Diels—Alder reactions and control the endo/exo selectivity. *ChemPhyschem* **2010**, *11* (1), 301–310.
- (18) Vogt, C.; Weckhuysen, B. M. The concept of active site in heterogeneous catalysis. *Nat. Rev. Chem.* **2022**, *6* (2), 89–111.
- (19) Ploense, L.; Salazar, M.; Gurau, B.; Smotkin, E. S. Proton Spillover Promoted Isomerization of n-Butylenes on Pd-Black Cathodes/Nafion 117. *J. Am. Chem. Soc.* **1997**, *119* (47), 11550–11551.
- (20) Sanabria-Chinchilla, J.; Asazawa, K.; Sakamoto, T.; Yamada, K.; Tanaka, H.; Strasser, P. Noble Metal-Free Hydrazine Fuel Cell Catalysts: EPOC Effect in Competing Chemical and Electrochemical Reaction Pathways. *J. Am. Chem. Soc.* **2011**, *133* (14), 5425–5431.
- (21) Neophytides, S. G.; Tsiplakides, D.; Stonehart, P.; Jaksic, M.; Vayenas, C. G. Non-Faradaic Electrochemical Modification of the Catalytic Activity of Pt for H<sub>2</sub> Oxidation in Aqueous Alkaline Media. *J. Phys. Chem.* **1996**, *100* (35), 14803–14814.
- (22) Cai, F.; Gao, D.; Zhou, H.; Wang, G.; He, T.; Gong, H.; Miao, S.; Yang, F.; Wang, J.; Bao, X. Electrochemical promotion of catalysis over Pd nanoparticles for CO<sub>2</sub> reduction. *Chem. Sci.* **2017**, 8 (4), 2569–2573.
- (23) Ryu, J.; Surendranath, Y. Polarization-Induced Local pH Swing Promotes Pd-Catalyzed CO<sub>2</sub> Hydrogenation. *J. Am. Chem. Soc.* **2020**, 142 (31), 13384–13390.
- (24) Westendorff, K. S.; Hülsey, M. J.; Wesley, T. S.; Román-Leshkov, Y.; Surendranath, Y. Electrically driven proton transfer

- promotes Brønsted acid catalysis by orders of magnitude. *Science* **2024**, 383 (6684), 757–763.
- (25) Wesley, T. S.; Román-Leshkov, Y.; Surendranath, Y. Spontaneous Electric Fields Play a Key Role in Thermochemical Catalysis at Metal-Liquid Interfaces. ACS Cent. Sci. 2021, 7 (6), 1045–1055.
- (26) Gorin, C. F.; Beh, E. S.; Kanan, M. W. An Electric Field–Induced Change in the Selectivity of a Metal Oxide–Catalyzed Epoxide Rearrangement. *J. Am. Chem. Soc.* **2012**, *134* (1), 186–189.
- (27) Gorin, C. F.; Beh, E. S.; Bui, Q. M.; Dick, G. R.; Kanan, M. W. Interfacial Electric Field Effects on a Carbene Reaction Catalyzed by Rh Porphyrins. *J. Am. Chem. Soc.* **2013**, *135* (30), 11257–11265.
- (28) Neophytides, S. G.; Tsiplakides, D.; Stonehart, P.; Jaksic, M. M.; Vayenas, C. G. Electrochemical enhancement of a catalytic reaction in aqueous solution. *Nature* **1994**, *370* (6484), 45–47.
- (29) Lim, C. W.; Hülsey, M. J.; Yan, N. Non-Faradaic Promotion of Ethylene Hydrogenation under Oscillating Potentials. *JACS Au* **2021**, 1 (5), 536–542.
- (30) Kaliyaraj Selva Kumar, A.; Zhang, Y.; Li, D.; Compton, R. G. A mini-review: How reliable is the drop casting technique? *Electrochem. Commun.* **2020**, *121*, 106867.
- (31) Chan, Y. Y.; Eng, A. Y. S.; Pumera, M.; Webster, R. D. Assessments of Surface Coverage after Nanomaterials are Drop Cast onto Electrodes for Electroanalytical Applications. *ChemElectrochem* **2015**, *2* (7), 1003–1009.
- (32) Li, H.; Buesen, D.; Williams, R.; Henig, J.; Stapf, S.; Mukherjee, K.; Freier, E.; Lubitz, W.; Winkler, M.; Happe, T.; Plumeré, N. Preventing the coffee-ring effect and aggregate sedimentation by in situ gelation of monodisperse materials. *Chem. Sci.* **2018**, 9 (39), 7596–7605.
- (33) Fuller, T. F.; Harb, J. N. Electrochemical Engineering; John Wiley & Sons, 2018; p 448.
- (34) Jackson, M. N.; Pegis, M. L.; Surendranath, Y. Graphite-Conjugated Acids Reveal a Molecular Framework for Proton-Coupled Electron Transfer at Electrode Surfaces. *ACS Cent. Sci.* **2019**, 5 (5), 831–841.
- (35) Fröhlich, H. Theory of Dielectrics: Dielectric Constant and Dielectric Loss; Clarendon Press, 1949.
- (36) Smith, J. M.; Van Ness, H. C.; Abbott, M.Introduction to Chemical Engineering ThermodynamicsMcGraw-Hill Education2005817
- (37) Eyring, H. Quantum Mechanics and Chemical Reactions. Chem. Rev. 1932, 10 (1), 103-123.
- (38) Walter, M.; Ramaley, L. Purification of acetonitrile. *Anal. Chem.* **1973**, *45* (1), 165–166.
- (39) Huckel, E.; Debye, P.Zur Theorie der Elektrolyte*Ergebnisse der Exakten Naturwissenschaften*SpringerBerlin, Heidelberg1924199–276
- (40) Boettcher, S. W.; Oener, S. Z.; Lonergan, M. C.; Surendranath, Y.; Ardo, S.; Brozek, C.; Kempler, P. A. Potentially Confusing: Potentials in Electrochemistry. ACS Energy Lett. 2021, 6 (1), 261–266
- (41) Mohandas, N.; Bawari, S.; Shibuya, J. J. T.; Ghosh, S.; Mondal, J.; Narayanan, T. N.; Cuesta, A. Understanding electrochemical interfaces through comparing experimental and computational charge density—potential curves. *Chem. Sci.* **2024**, *15* (18), 6643—6660.
- (42) Yu, K.; Kumar, N.; Aho, A.; Roine, J.; Heinmaa, I.; Murzin, D. Y.; Ivaska, A. Determination of acid sites in porous aluminosilicate solid catalysts for aqueous phase reactions using potentiometric titration method. *J. Catal.* **2016**, 335, 117–124.
- (43) Banks, C. E.; Crossley, A.; Salter, C.; Wilkins, S. J.; Compton, R. G. Carbon Nanotubes Contain Metal Impurities Which Are Responsible for the "Electrocatalysis" Seen at Some Nanotube-Modified Electrodes. *Angew. Chem., Int. Ed.* **2006**, 45 (16), 2533–2537.
- (44) Domagala, K.; Borlaf, M.; Traber, J.; Kata, D.; Graule, T. Purification and functionalisation of multi-walled carbon nanotubes. *Mater. Lett.* **2019**, 253, 272–275.
- (45) Kruusma, J.; Mould, N.; Jurkschat, K.; Crossley, A.; Banks, C. E. Single walled carbon nanotubes contain residual iron oxide

impurities which can dominate their electrochemical activity. *Electrochem. Commun.* **2007**, *9* (9), 2330–2333.